




Article

Study on the Degradation Pattern of Impact Crater Populations in Yutu-2's Roving Area

Xinyu Ma ¹, Meixi Chen ¹, Teng Hu ^{1,2,*}, Zhizhong Kang ^{1,2}  and Meng Xiao ¹

¹ School of Land Science and Technology, China University of Geosciences, Beijing 100083, China; 1012214108@email.cugb.edu.cn (X.M.); 1012214109@email.cugb.edu.cn (M.C.); zzkang@cugb.edu.cn (Z.K.); 2012210008@email.cugb.edu.cn (M.X.)

² Subcenter of International Cooperation and Research on Lunar and Planetary Exploration, Center of Space Exploration, Ministry of Education of the People's Republic of China, Beijing 100083, China

* Correspondence: huteng@cugb.edu.cn

Abstract: A detailed analysis of the panoramic camera data from the 27th to 33rd lunar days was conducted on the high-resolution scenes captured by the Yutu-2 rover stations. This analysis aimed to determine the detailed morphological parameters of the 2015 impact craters within the inspection area. The levels of degradation observed in the impact craters were determined alongside the surface features. Subsequently, the degradation patterns of the impact craters located within the Yutu-2's roving area and the distribution patterns of the morphological parameters were analysed and investigated. The results of the analysis indicate that 94% of the impact craters exhibited severe degradation, 80% had depth-to-diameter ratios (DDRs) ranging from 0.07 to 0.17, and the remaining craters were moderately degraded. The DDRs of the impact craters exhibited a declining trend with an increase in the dimensions of the impact craters. Additionally, the degree of degradation of impact crater populations demonstrated a decreasing trend. In general, the impact craters along the rover's route exhibited severe degradation, with the population of degradation degrees gradually decreasing with increasing diameter.



Citation: Ma, X.; Chen, M.; Hu, T.; Kang, Z.; Xiao, M. Study on the Degradation Pattern of Impact Crater Populations in Yutu-2's Roving Area. *Remote Sens.* **2024**, *16*, 2356. <https://doi.org/10.3390/rs16132356>

Academic Editors: Jianguo Yan and Giancarlo Bellucci

Received: 9 May 2024

Revised: 20 June 2024

Accepted: 24 June 2024

Published: 27 June 2024



Copyright: © 2024 by the authors. Licensee MDPI, Basel, Switzerland. This article is an open access article distributed under the terms and conditions of the Creative Commons Attribution (CC BY) license (<https://creativecommons.org/licenses/by/4.0/>).

Keywords: Yutu-2; rover images; impact craters; crater degradation patterns; the Moon

1. Introduction

Yutu-2 travelled to the Von Karman impact crater in the South Pole-Aitken Basin at the lunar south pole and has been used for lunar surface roving [1–3]. The paucity of sub-metre-scale impact crater data and related studies is a consequence of the resolution of orbiter images, which is limited to 0.5 m/pixel. The panoramic camera on the Yutu-2 rover, with the detection advantage of in situ close-range observation, provides valuable technical data for extracting the morphological parameters of sub-metre-scale impact craters, analysing the three-dimensional scene, and examining the pattern of the group's morphological characteristics [4]. The images record impact craters, with diameters ranging from sub-metre to metre, providing a data basis for studying the formation, degradation, and flux of sub-metre-scale impact craters. They are also significant for revealing the population patterns of these impact events on the lunar surface.

The degradation state of impact craters directly characterizes the age of their formation. Consequently, the morphology of impact craters changes over time, and it is indicative of the evolution and age of the lunar surface stratigraphy [5,6]. Morphology/age relationship analysis is the main research method used by most scholars to study the degradation pattern of impact craters based on morphological features. For example, Craddock (1972) and Haruyama et al. (2004) studied the degradation process of impact craters and described the relative age of geological units via the degradation parameter [7,8]; Wood (1977) and Ivanov et al. (2002) classified the degradation grade through the morphology of impact craters [9,10], and Craddock (1972) established a degradation model

and estimated the degradation and erosion rate of impact craters using the Clementine data [7]. Research on the saturation equilibrium state of the impact crater density is ongoing. Hartman (1997) and James (2009) studied the equilibrium state of the impact crater distribution using computer modelling methods [11,12]. Li Kun (2013) employed the data on impact craters in the typical Moon Sea area to investigate the morphology of the impact craters. He began by examining the degradation of the impact craters and then proceeded to identify the impact crater depth as a parameter for determining the degradation. The relationship between the production and chronological functions of the impact craters was employed to derive the time-series curves of ascending readings of impact crater size and establish the degradation model [13]. Previous studies have demonstrated that for impact craters of a similar size, the older the formation age is, the more apparent the degradation phenomenon is, and the smaller the scale of the impact crater is, the greater the probability of its disappearance is due to the effects of degradation.

Statistical studies on the morphology of degradation grades and other related features are of significant importance in order to gain an understanding of the correlation between the morphological evolution of impact craters and the age of the corresponding lunar surface in that region. The current methods for grading the degradation of impact craters are predominantly based on visual interpretation. In 1963, Arthur proposed four degradation types for the moon. The classification system proposed by Arthur comprises four classes, designated C1, C2, C3, and C4. C1 refers to fresh impact craters; C2 to initially degraded impact craters; C3 to impact craters with a severely eroded morphology; and C4 to completely flattened impact craters [14]. The studies by McGill and Wise (1972) and Basilevsky et al. (1976) proposed five degradation types for the moon. These were classified into three main classes—A, B, and C—and two transitional classes—AB and BC. The classes A, B, and C are used to indicate the following: Class A indicates a fresh impact crater, Class B indicates an initially degraded impact crater (with a smooth rim), and Class C indicates a completely flattened impact crater [15,16]. In order to study the morphological grading of impact craters, Yao Meijuan et al. (2016) employed the optimal grading method which involved the optimal division of diameters, resulting in 10 grades [17]. Overall, the statistics analysis of features related to the degradation level of impact craters is primarily based on orbiter image data with a limited image resolution. Furthermore, the dimensions of the extracted and analysed impact craters are relatively considerable, which makes it challenging to obtain the availability of in situ validation data on the lunar surface.

Given the characteristics of Yutu-2's data, we employed the rover's image data to construct a high-resolution three-dimensional scene of the roving area and generated a digital elevation model (DEM) and digital orthophoto model (DOM). Subsequently, the impact craters were manually extracted and identified all the impact craters in the images using the automatic extraction method for the impact craters' morphological parameters. This resulted in the accurate determination of the depth, diameter, and other morphological parameters for the identified impact craters. The degradation levels were classified according to the texture characteristics of the impact craters, and the degradation patterns of the impact crater groups in the patrol area and the distribution patterns of the morphological parameters were studied and analysed.

Section 2 presents the experimental data and data processing methods employed in this study. Section 3 presents the results of the manual identification of the impact craters along the rover's route and analyses their degradation. Section 4 presents a discussion and analysis of the degradation and degradation patterns of the population of small impact craters in the roving area, with a comparison to the existing data on the impact craters along the rover's route and the data on Chang'e-4's landing area.

2. Data and Methodology

2.1. Data

We used the DEM and DOM images produced by Yutu-2's panoramic camera [18] as the image data and assigned geo-referenced coordinates (GCS_Moon_2000). The resolutions

of DEM and DOM images are variable, with a resolution of 0.0011 m at close range and 0.004 m at longer range. The panoramic camera is equipped with two imaging modes: colour imaging and panchromatic imaging. These modes can be switched between the two modes during the shooting process. The image resolutions of the colour mode and the panchromatic imaging mode are 2352×1728 pixels and 1176×864 pixels, respectively. The camera's field-of-view angle is $19.6^\circ \times 14.5^\circ$ [19]. The panoramic camera is designed to capture 360° images around the station by utilising the mast's up-down and left-right rotation. A total of 56 images can be captured in each turn, including 28 pairs of images in different directions at two altitude angles. Figure 1 displays a section of imagery captured by a panoramic camera. This enables the three-dimensional stereo imaging of the topography and landscape of the landing and roving areas [20]. Consequently, the panoramic camera on Yutu-2 can achieve clear imaging from the foot of the rover to the farthest point in the field of view, with a spatial resolution can reach the millimetre scale during close observation. As of 20 September 2023, the Chang'e-4 mission has completed its 62nd lunar day. The study utilised data from the panoramic camera images captured between the 27th and 33rd days of the lunar days.

2.2. Methodology

The panoramic camera images captured by Yutu-2 were processed to obtain the DEM and DOM images. Impact craters were then manually extracted from the images using algorithms to correct the centre of the extracted impact craters and extract the required morphological parameters. Subsequently, the degradation grades were classified in conjunction with the spatial morphology of the impact craters. Finally, the degradation grades and the corresponding morphological parameters of the craters were employed to conduct a study of the degradation patterns of the impact craters and the distribution patterns of the morphological parameters on the backside of the moon. The research method is illustrated in Figure 2.

2.2.1. Image Processing

The panoramic camera images were subjected to three processing stages. Firstly, the images were classified according to the time of shooting and divided into 10 stations, each including 122 image data. The images from each station were imported into the MetashapePro 1.7.4 software (<https://www.agisoft.com/zh-cn/downloads/installer/>, accessed on 21 March 2023) for processing. This involved camera calibration, scale scaling, and other procedures, resulting in the creation of a dense point cloud. The focal length and pixel size of panchromatic camera were 50.29 mm and 0.0148 mm, respectively, while those of the colour camera were 50.274 mm and 0.0074 mm. Both colour and panchromatic images were employed in the reconstruction of three-dimensional scenes and the generation of digital elevation models and digital orthophoto models. The scale scaling was calibrated based on the standard of Yutu-2's track, which was determined to be 15 cm. Finally, a grid image using the dense point cloud was generated to produce the DEM and DOM images, and the 3D model and corresponding texture were obtained simultaneously.

2.2.2. Impact Crater Identification

Impact craters have depressed circular features, so they are identified based by the contrast between light and dark features under lighting conditions. In this study, the impact craters in the generated DOM and DEM images were identified and marked using the CraterTools software (<https://www.geo.fu-berlin.de/en/geol/fachrichtungen/planet/software/index.html>, accessed on 2 June 2023).

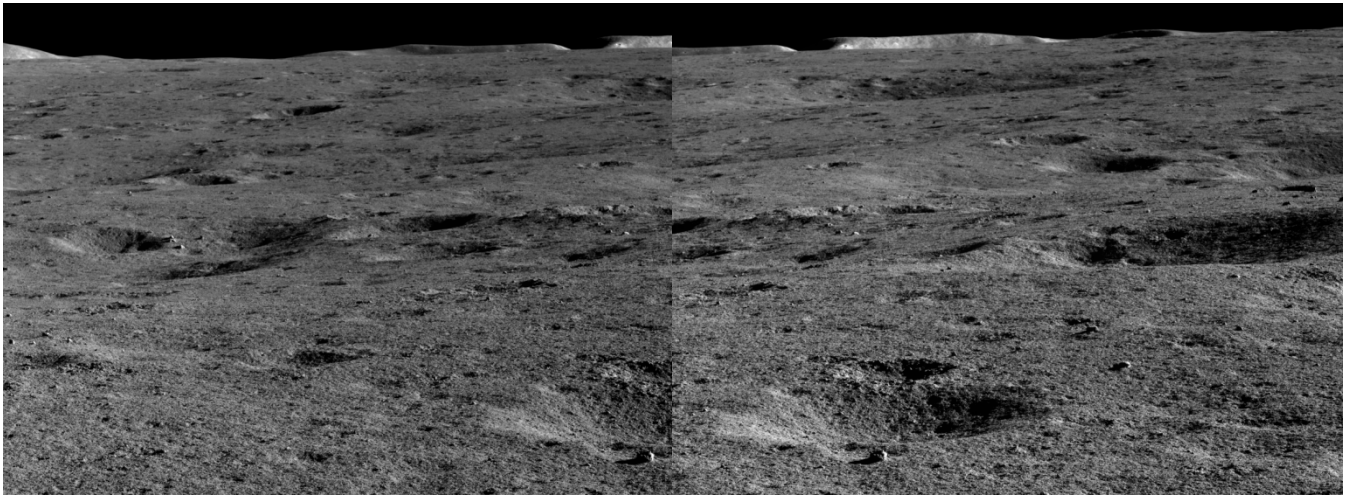


Figure 1. Parts of an original panoramic camera image.

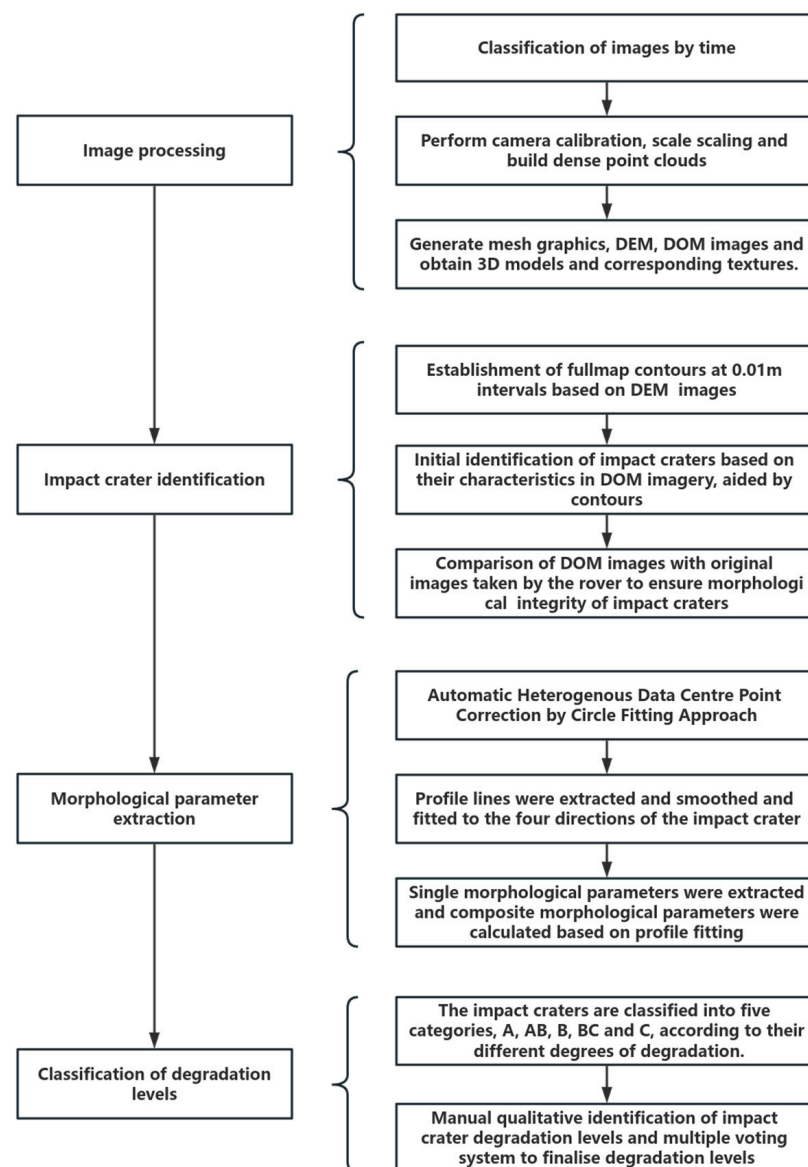


Figure 2. Step diagram of data processing.

We adopted a multi-source determination method in the identification process, as shown in Figure 3. Figure 3a shows the identification of impact craters in the DOM images based on the depressed circular and light–dark contrast features. Due to the limited field of view of the panoramic camera, some impact craters were not photographed all the way to the bottom. These incomplete craters were discarded in the identification process. The metre-scale impact craters were generally small-sized with shallow depths, resulting in a lack of obvious light–dark contrast, which cannot be quickly identified from the DOM images alone. To solve this problem, we created full map contours based on the DEM images to assist in the impact crater identification with the DOM images (with 0.01 m contour intervals). Figure 3b shows the impact craters identified based on the contours. The integrity of the fit in the centre of the impact crater cannot be clearly seen due to the impact of the resolution of the DOM image. Therefore, when identifying the impact craters, the DOM image was compared with the original rover image to ensure that the impact crater’s morphology was complete. Figure 3c shows the original rover image of the rover corresponding to Figure 3a.

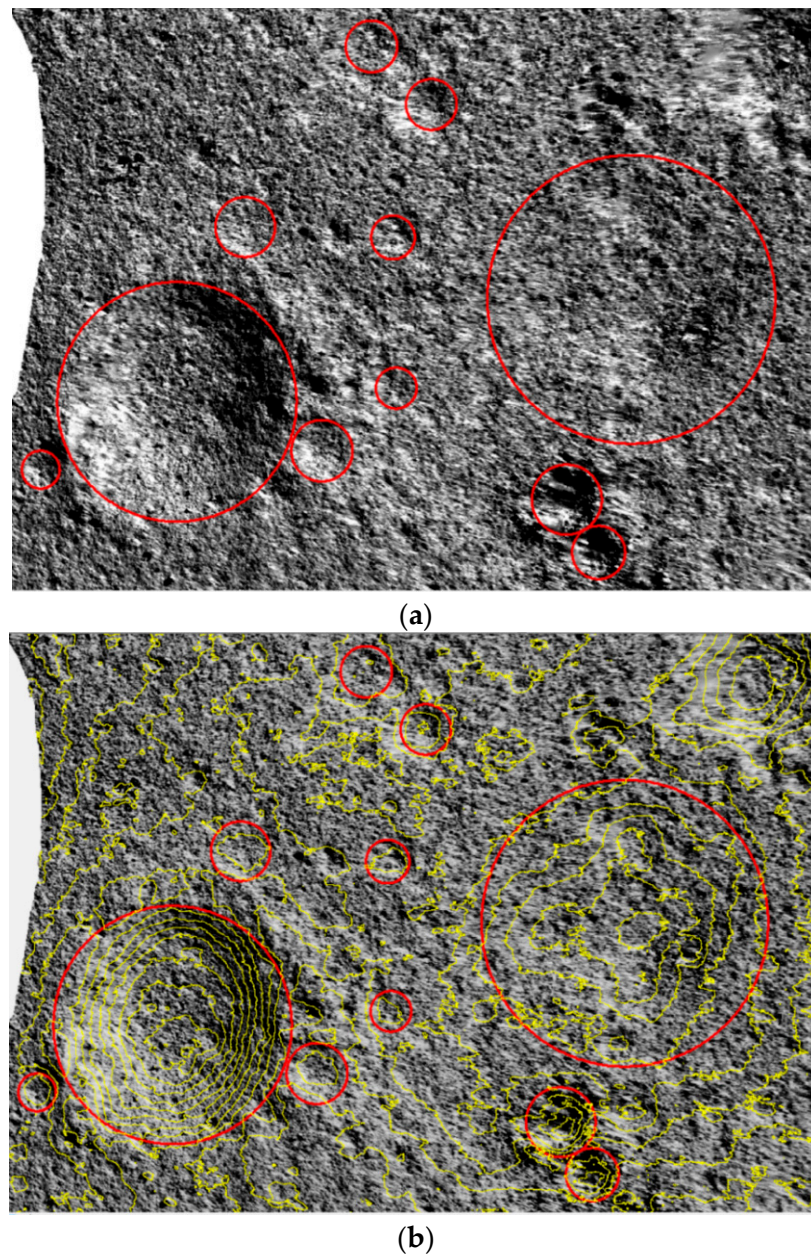
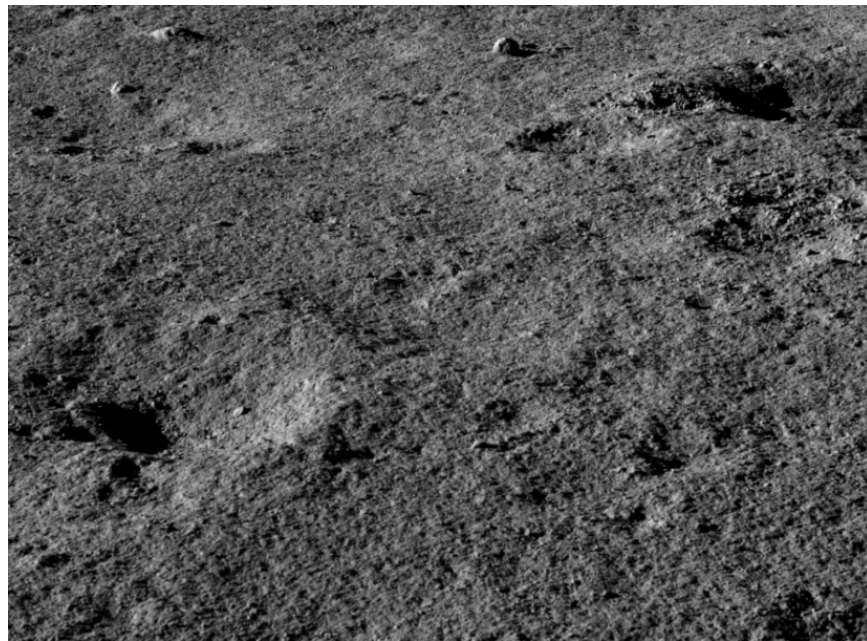


Figure 3. Cont.



(c)

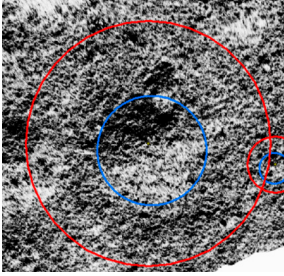
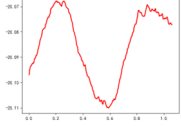
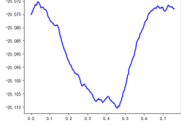
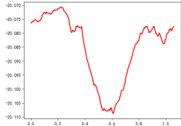
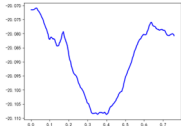
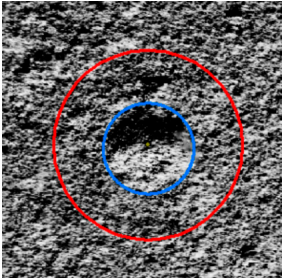
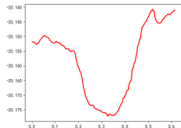
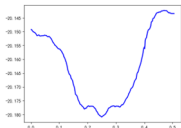
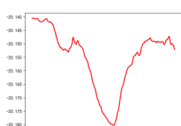
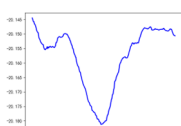
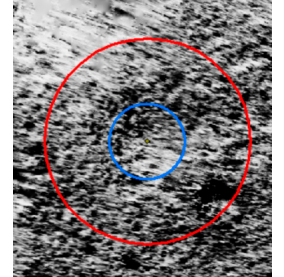
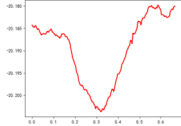
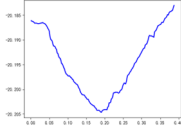
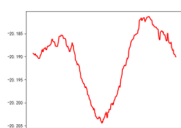
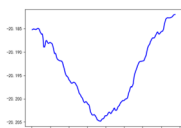
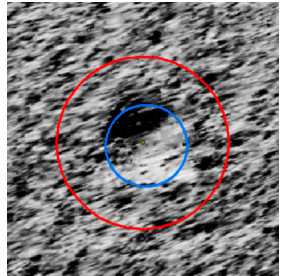
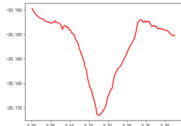
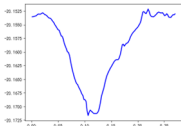
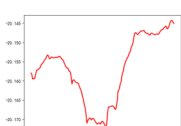
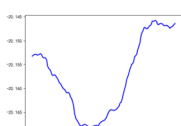
Figure 3. Impact crater identification method. (a) Impact crater marking with DOM as base map. (b) Contour-assisted recognition with DOM as base map. (c) Visual comparison of the original images of the rover. The red circle in the figure shows the approximate location of the impact crater, and the yellow line shows the contour lines.

2.2.3. Morphological Parameter Extraction

Since contours or elevation differences are not easily identifiable, it is possible to use an algorithm accurately calculate the peak locations to find the exact edges of impact craters and fit them to the actual centre. Therefore, after roughly extracting these impact craters, we used an algorithm to centre correct the extracted impact craters to find the correct location and extent of the impact craters, and based on this, we extracted the morphological parameters.

We used an automatic extraction algorithm to extract polymorphic parameters of the impact craters. The algorithm first corrected the offset problem of the centre point offset problem via circle fitting, so that the offset centre point was closer to the actual centre position of the impact crater. The aim of the algorithm was to automatically correct the centre point of the impact crater data from heterogeneous sources, to resolve the coordinate bias between these data, and to improve the data quality. A comparison of the results before and after the centre correction is shown in Table 1. The least squares algorithm was used to fit high order polynomials to the profile lines in the four directions of the impact craters. The higher order polynomial functions of the profile lines with a better fit were obtained to generate the fitted profile lines and polynomial models to describe the morphology of the impact crater profiles based on the mathematical and theoretical dimensions. Finally, eight morphological descriptors were designed, including individual and composite morphological parameters (including depth, internal and external slope, pit lip width, pit lip height, etc.) and composite morphological parameters (including roundness, the depth-to-diameter ratio, and the body shape ratio). In this paper, we mainly studied morphological parameters such as diameter, depth, and depth-to-diameter ratio, which can reflect the impact craters' shape, size, and evolution of impact craters.

Table 1. Before and after correction of impact crater centres. In the figure, red represents the position and profile line of the impact crater after the central correction, while blue represents the position and profile line before the central correction. In the table, X and Y represent the horizontal and vertical profile lines relative to the impact crater. The extraction process involves four directions, but only two are shown in this table. The horizontal and vertical axes of the profile map are all in meters.

Comparison of Centre Point Correction before and after	Profile Line Aspects	After Centre Point Correction	Before Centre Point Correction
	X		
	Y		
	X		
	Y		
	X		
	Y		
	X		
	Y		

2.2.4. Classification of Degradation Levels

According to McGill and Wise (1972) and Basilevsky et al. (1976) [15,16], impact craters are classified into five classes, namely A, AB, B, BC, and C, according to their different degrees of degradation. Category A indicates the freshest impact craters, while category C indicates the most degraded impact craters. However, while previous studies have focused on craters larger than a few tens of metre in diameter, this study focuses on sub-metre craters. The data used in this study have a higher resolution and show more detailed impact crater morphology than the satellite observations used by previous authors. The impact craters in this study are therefore categorized according to the descriptions of each type in previous studies. Figure 4 shows examples of impact craters with different types

of degradation: the Class A fresh impact craters have obvious bright or clear edges, large impact crater depths, and sharp contrasts between light and dark; the Class AB impact craters are slightly degraded, with more obvious contrasts between light and dark; the Class B impact craters have clear and intact edges, with traces of degradation, and obvious shadows; the Class BC impact craters have incomplete edges, with obvious degradation, and shallow depths with minor differences between light and dark; and the Class C impact craters have very faint and incomplete edges, severe degradation, shallow impact crater depths, and basically no shadows, and circular contours are visible when the image is stretched.

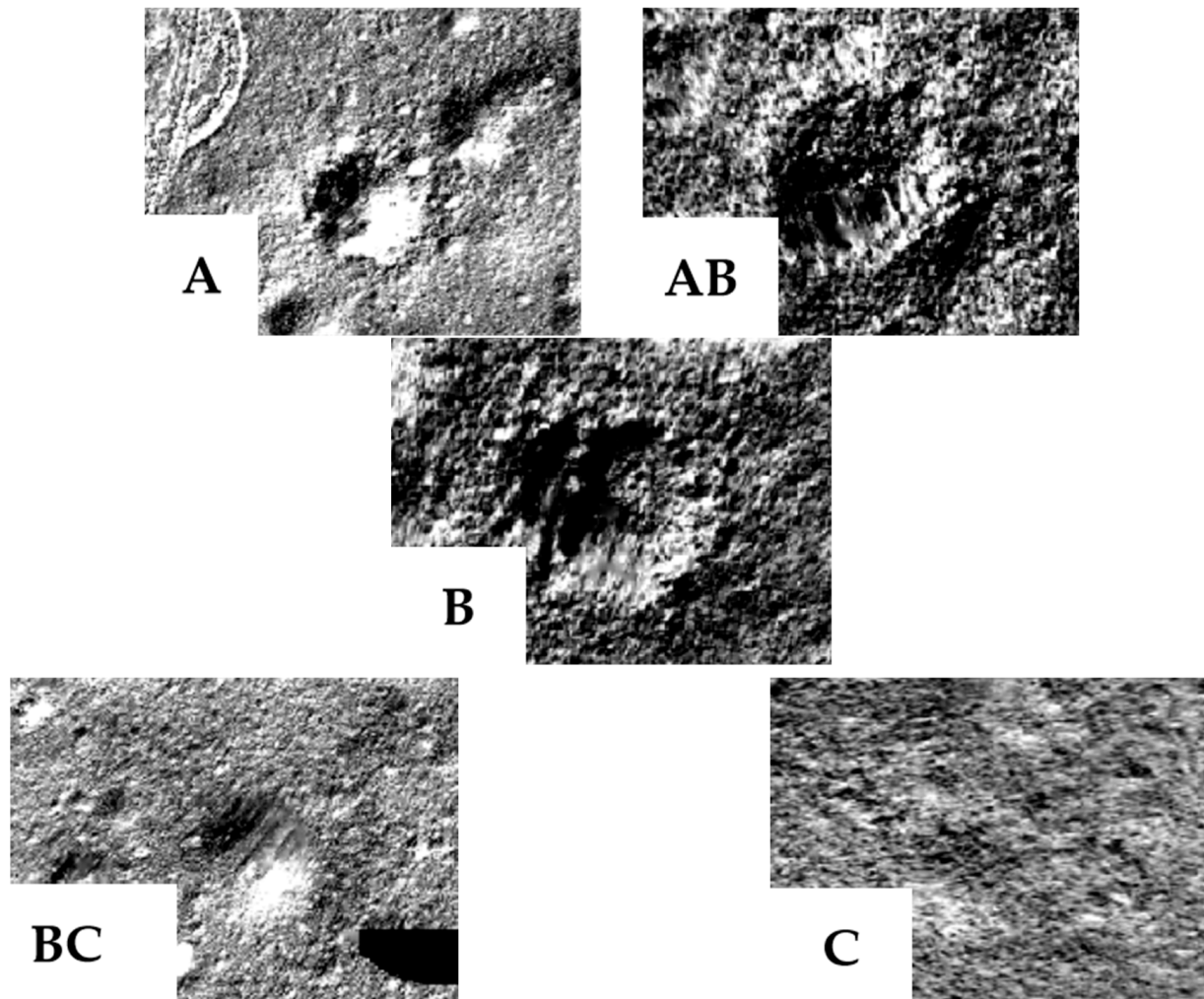


Figure 4. Examples of different types of impact crater degradation. The diagram shows the degradation levels of the impact crater. The levels are marked in the lower left corner.

We used manual qualitative identification of the impact crater degradation classes. Manual qualitative classification usually introduces human subjective factors, so errors in judgement are inevitable. For example, the Class BC impact craters in Figure 4 are similar to Class C impact craters and can be classified. Therefore, a multi-voting procedure was applied to all impact craters, where all impact craters were first assigned degradation classes by three researchers each. The resulting degradation classes of the impact craters were then summarized. If the degradation class of an impact crater was disputed, the three researchers discussed its degradation class based on the DOM image, original images, and other supporting data. In the end, the degradation classes of all impact craters were agreed upon by all, and the classification of impact crater degradation classes was completed.

3. Results

We carried out artificial identification and morphological parameter extraction for the impact craters photographed during the Yutu-2 rover's journey using the research methods described above. We then performed statistics and analysis on the degree of degradation.

3.1. Results of Impact Crater Extraction

We carried out scene reconstructions and generated DEM and DOM images for 10 stations based on Yutu-2's panoramic camera images, as shown in Figure 5. The DEM and DOM images were generated from the foot of the rover to approximately 10 m from the rover. Both the DEM and DOM images resolutions are variable values, with a resolution of 0.0011 m at close range and 0.004 m at longer range. The results demonstrate the high image resolution and high integrity of the impact crater images, which provided a good basis for the study of the impact craters in Yutu-2's orbit.

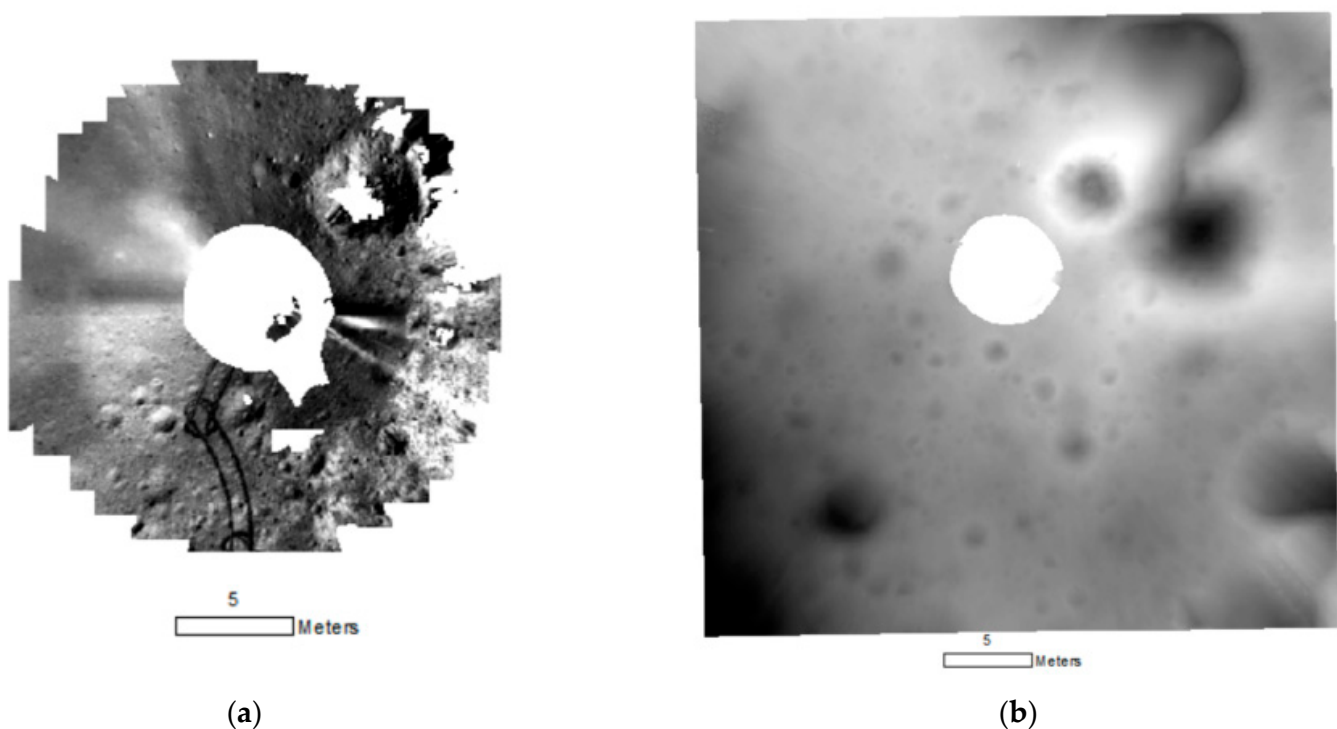


Figure 5. Generated images: (a) DOM image; (b) DEM image.

In this study, the DOM image of each station served as the basic study area. The specific study area was an annular area with an average outer and inner diameter of 11 m and 3 m, respectively, centred on the rover position. The largest and smallest outer diameters were 16 m and 9 m, respectively, as shown in Figure 6. The distribution of the impact craters in the DOM image is shown in Figure 7, where the impact craters are distributed in a radial pattern around the rover. The further away from the rover, the lower the density of impact craters that could be identified. A small number of complete impact craters were distributed outside the DOM image. The majority of impact craters were small, with the highest concentration near the centre of the rover. The distribution pattern of all the impact craters extracted from the ten stations was found to be consistent with that shown in Figure 7.

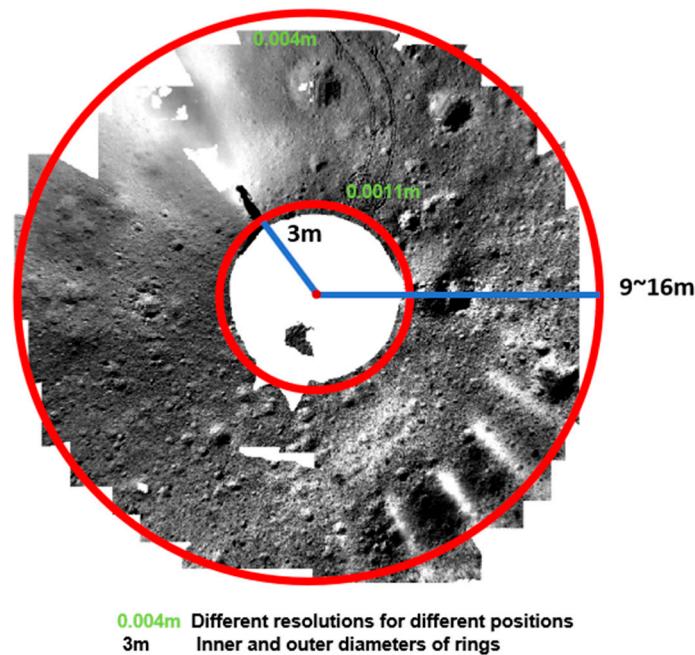


Figure 6. Schematic of DOM image range. The red ring in the figure represents the effective range of the image, and the meanings represented by the other colours are marked in the figure.

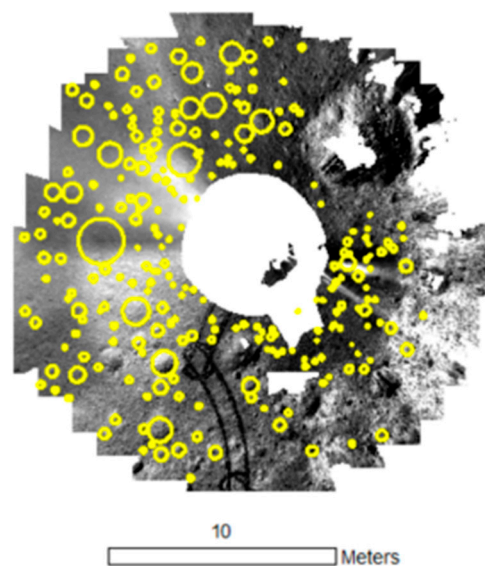


Figure 7. Distribution of impact craters in DOM images. The yellow circles represent the approximate locations of all extractable impact craters at the station in the diagram.

A total of 2110 impact craters were identified based on the DEM and DOM images. Some impact craters were not captured at the bottom due to the angle limitations of the panoramic camera. A comparison was made between the identified impact craters and the original images captured by the panoramic camera. Those the impact craters that were not photographed at the bottom were excluded. A total of 2015 complete impact craters were extracted. This result ensured the completeness of the impact crater data and furnished a robust foundation basis for the subsequent degradation parameter extraction, class classification, and statistical analysis.

The diameters of all impact craters at the ten stations were enumerated. The smallest impact crater diameter was 0.098 m, the largest was 4.077 m, and the mean value was 0.503 m. There were 19 impact craters with diameters greater than 2 m, 151 with diameters

greater than 1 m, and 79 with diameters less than 0.2 m. Figure 8 presents the size–frequency statistics of the impact craters with diameters of less than 2 m. The impact craters with diameters between 0.2 and 0.3 m exhibited the highest frequency, reaching 504, followed by those between 0.3 and 0.4 m, with a frequency of 466. The majority of the impact craters (over 80%) were concentrated in the diameter range of 0.2–0.8 m, with the 0.2–0.5 m range accounting for 64.4%. The data set primarily comprised sub-metre impact craters were extracted. The impact craters were numerous and concentrated in size, with a gradual increase infrequency as their diameters decreased with diameters below 2 m.

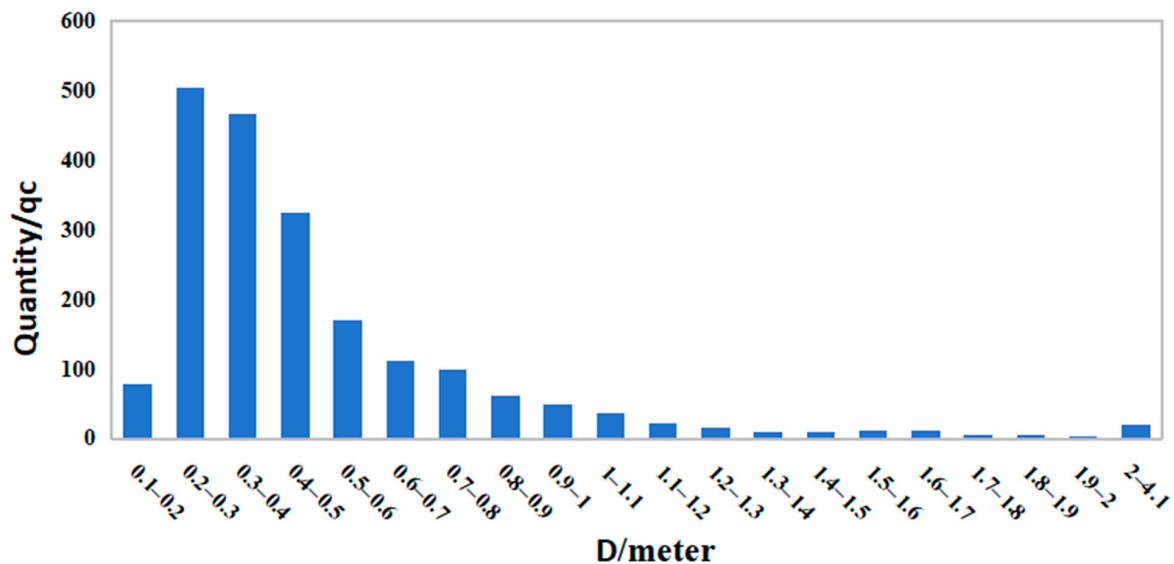


Figure 8. Size–frequency distribution of the impact craters up to 2 m in diameter.

3.2. Results of Morphological Parameter Extraction for Impact Craters

The depth and depth-to-diameter ratio parameters of the impact craters were extracted from the available impact crater information and subjected to statistical analysed.

Figure 9 presents the linear depth–diameter relationship, with a correlation coefficient exceeding 0.7 and high credibility. The depth-to-diameter ratios of the impact craters with a diameter of more than 2 m did not exceed 0.16, while those of impact craters with a diameter of less than 2 m were concentrated in the range of 0.05 to 0.20. The small size of the impact craters resulted in their generally small diameters and depth-to-diameter ratios.

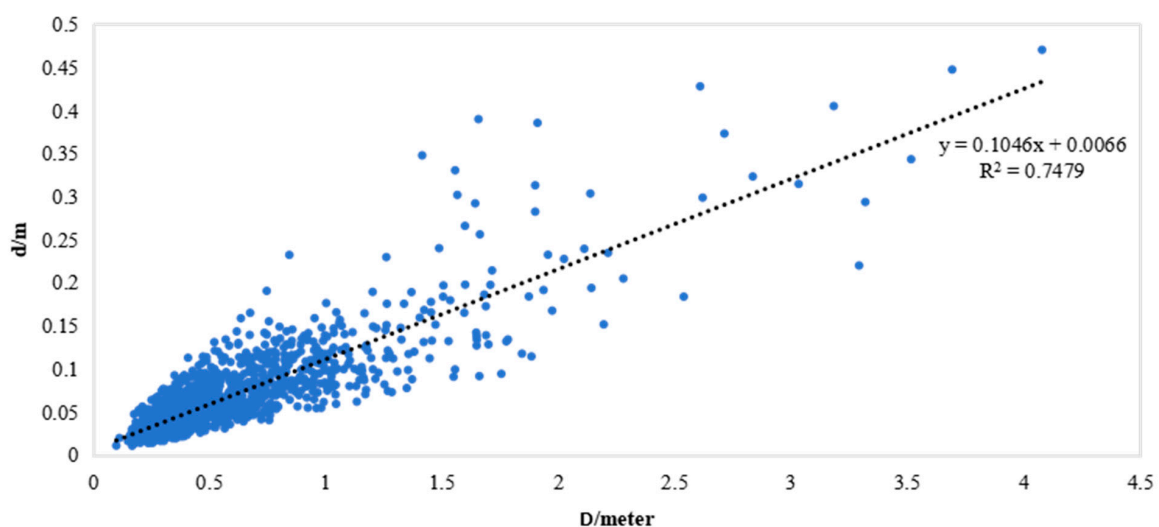


Figure 9. Depth–diameter relationship.

Figure 10 presents the frequency statistics of the depth-to-diameter ratio. The depth-to-diameter ratios of the impact craters exhibited a normal distribution, with values ranging from 0.053 and 0.29, a mean of 0.122, and a variance of approximately 0.039. The depth-to-diameter ratios were found to be concentrated in the range from 0.07 to 0.17, with more than 80% of the data falling within this range. Furthermore, 50% of the impact craters exhibited depth-to-diameter ratios in the range from 0.09 to 0.13.

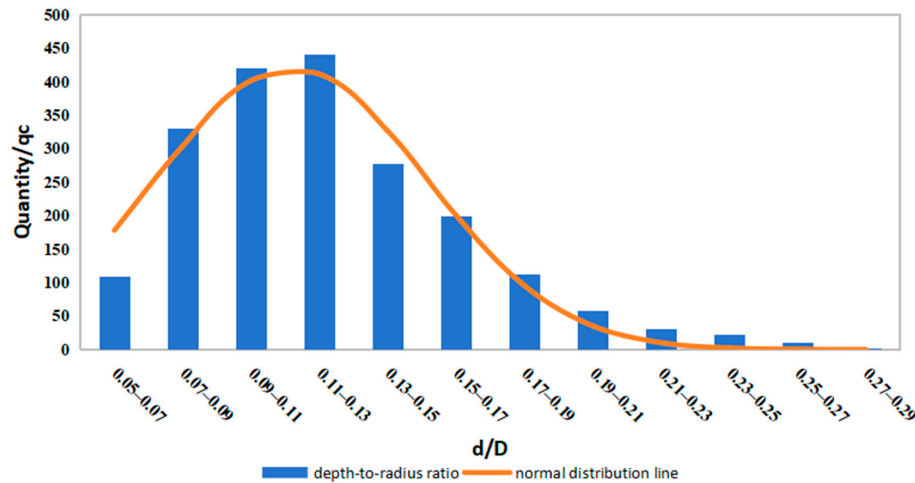


Figure 10. Frequency plot of depth-to-diameter ratios.

The relationship between the diameter and depth of an impact crater is depicted in Figure 11. The impact crater depth–diameter ratio values were distributed across a range of diameter segments from 0.1 to 2 m. The minimum depth–diameter ratio value was close to 0.06. The impact craters with diameters of less than 1 m exhibited a maximum depth–diameter ratio value of greater than 0.25. The maximum difference in the depth–diameter ratios was observed in the diameter range of 0.4 to 0.5 m. The mean value of the depth-to-diameter ratio was 0.22. The median and mean values of the depth-to-diameter ratio demonstrated a general downward trend with increasing diameter, although this decline was not particularly pronounced. The depth-to-diameter ratio values exhibited a notable increase increased at diameters of 1.4–1.5 m and 1.9–2.0 m. This may have been an inadvertent consequence of the limited data on impact craters with diameters of exceeding than 1 m. Overall, there was some variation in the depth-to-diameter ratio with diameter. The depth-to-diameter ratios of the impact craters with diameters below 2 m exhibited a decreasing trend with increasing size, although the degree of decrease was insignificant.

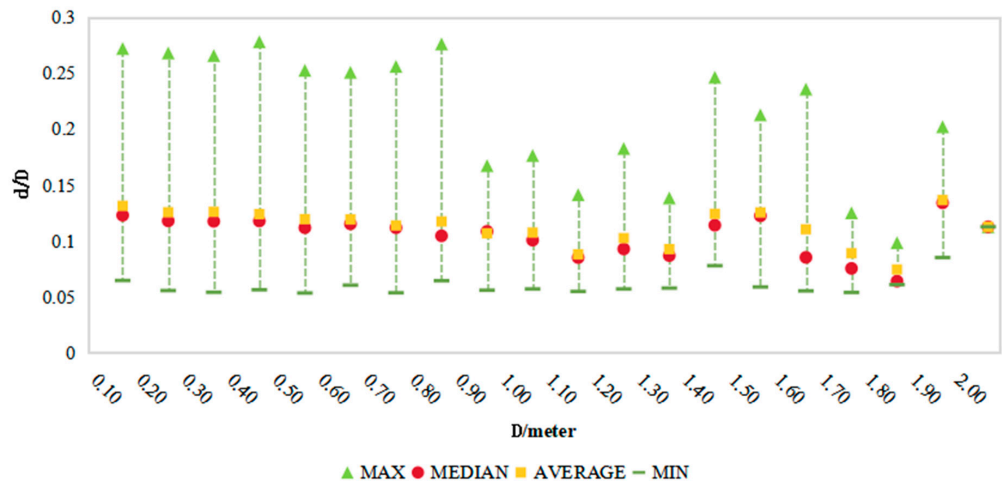


Figure 11. Diameter–depth ratio relationship.

3.3. Results of Impact Crater Degradation Classification

The degradation levels of the 2015 impact craters were obtained following the voting classification of the impact craters. The percentages are shown in Figure 12. There were no Class A and AB impact craters. Meanwhile, there were 1229, 686, and 100 Class C, BC, and B impact craters, accounting for 60%, 34%, and 6%, respectively. This indicates that the extracted impact craters at the 10 stations were mostly Class BC and C, exhibiting morphology that is not readily identifiable and a high degree of degradation.

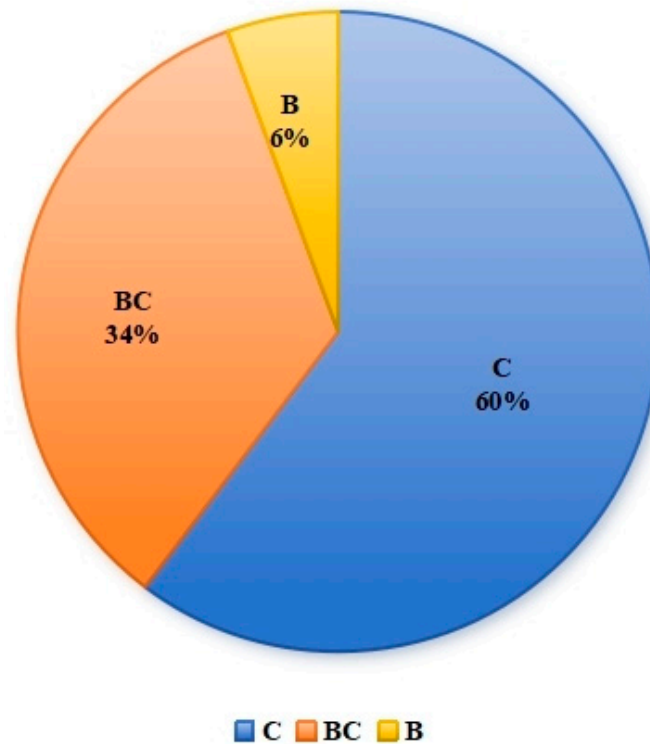


Figure 12. Degradation level classifications as percentages.

The relationship between the diameter of impact craters and their degradation is illustrated in Figure 13. The majority of Class C impact craters exhibited a high percentage (greater than 50%) in the majority of the diameter bands. The median diameters of the Class B, BC and C impact craters were 0.29 m, 0.35 m, and 0.42 m, respectively. The degradation level of the Class B impact craters in the size intervals of 0.1–0.5 m, 0.5–1 m, 1–1.5 m, and 1.5–2 m, varied in ratio from 5.83% to 3.67%, 2.11%, and 0%; that of Class BC impact craters varied from 37.32% to 26.88%, 32.63%, and 21.62%; and that of Class C impact craters changed from 56.85% to 69.45%, 65.26%, and 78.38%. The statistical analysis indicates show that the degradation of the small impact crater group was significant, with the majority impact craters formed by the impact of small objects on the lunar surface. The limited energy of these impacts prevented the occurrence of a violent melting process in the material, which, in turn, limited the size of the formed craters. In addition, the material strength of the walls of these craters was lower than that of large craters, making them susceptible to degradation. However, the presence of impact craters with diameters less than 1 m diameter with Class B degradation indicated that the small impact craters had both severely and moderately degraded parts. This, in turn, indicated that the small impact craters had a low degree of solidity and were easily degraded and that fresh impact craters could easily be generated under the influence of external forces and other factors, while the original impact craters were continuously degraded.

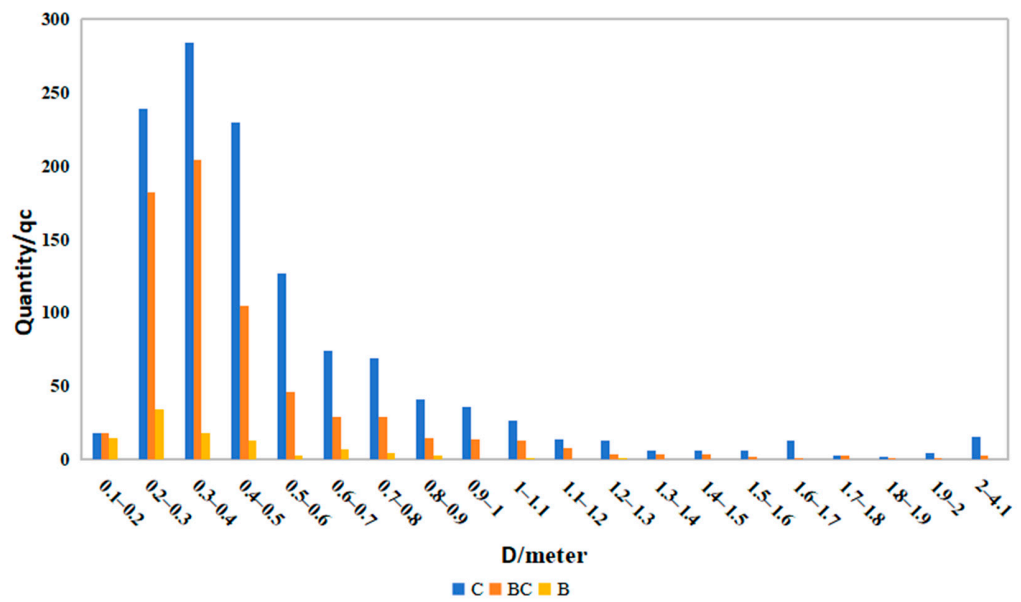


Figure 13. Diameter–degradation level relationship.

The relationship between impact crater depth and degradation class is shown in Figure 14. The average depth-to-diameter ratios of Class C, BC, and B impact craters were 0.112, 0.132, and 0.165, respectively, with 80% of the Class C impact craters having depth-to-diameter ratios in the range of 0.053–0.153; 80% of the Class BC impact craters having ratios in the range of 0.073–0.173; and 80% of the Class B impact craters having ratios in the range of 0.093–0.213. Overall, the ratios of the Class C impact craters increased and decreased with the increasing in the depth-to-diameter ratio, changing from 83.44% to 75.21%, 68.26%, 57.58%, 50.54%, 45.30%, 37.37%, 32.00%, 30.00%, 28.57%, 0.00%, 0.00%, and 0.00%, respectively. The ratio of Class B impact craters gradually increased from 0.63% to 0.85%, 3.42%, 4.55%, 7.73%, 17.17%, 22.00%, 26.67%, 28.57%, 55.56%, and 50.00%, showing that the number of impact craters with severe degradation increased as the depth-to-diameter ratio decreased.

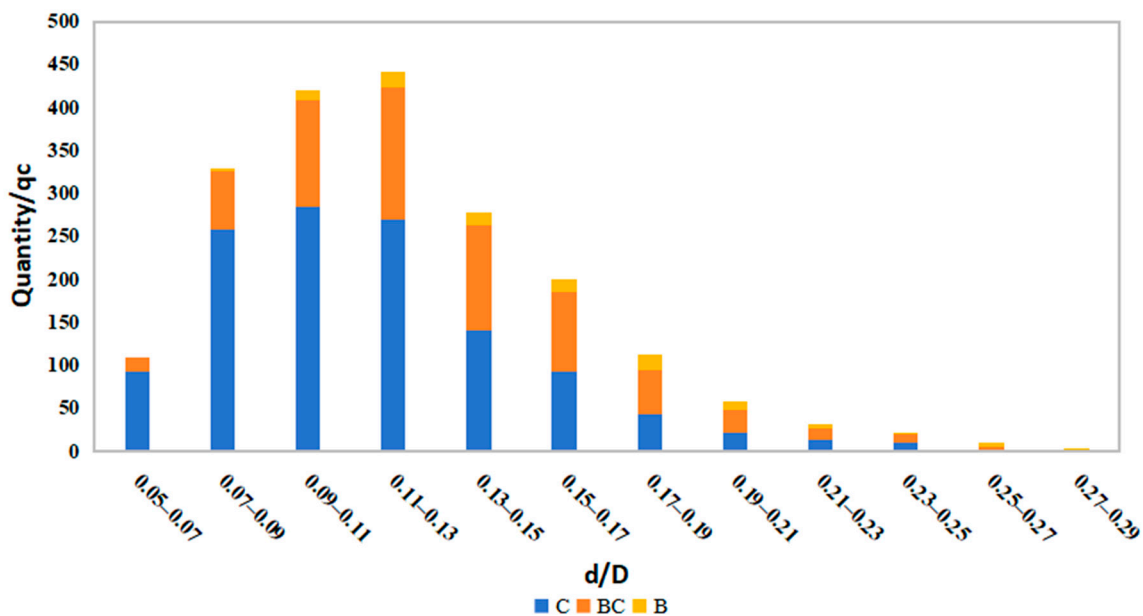


Figure 14. Relationship between depth-to-diameter ratio and degradation classification.

4. Discussion and Analysis

4.1. Comparison with Available Results

Yang et al. (2021) [21] studied sub-metre impact craters. In the statistical results of diameter–frequency, only 12 of the 371 impact craters had a diameter larger than 1 m, and more than 50% had a diameter of 0.1–0.3 m. In this paper, the statistical results of the 2015 impact craters show that 80% of the impact craters in the study area had a diameter concentrated in the range of 0.2–0.5 m, with a total of 1294. A total of 151 impact craters had diameters larger than 1 m, accounting for 7.4%. Compared to existing results, this study extracted a larger number of impact craters was extracted in this study, and the results are more general. However, the size of the impact craters was concentrated in the range of 0.1–2 m, and impact craters with sizes below 0.1 m and larger than 2 m were missing.

The frequency statistics of the depth-to-diameter ratios of 63 impact craters presented by Yang et al. (2021) [21] (Figure 15) revealed depth-to-diameter ratios ranging from 0.03 to 0.18, with a mean value of 0.12 and a variance of 0.03. A total of 78% of the impact craters exhibited depth-to-diameter ratios between 0.10 and 0.16. The statistical analysis of the data revealed that the depth-to-diameter ratios of the impact craters in the study area exhibited a wide distribution, ranging from 0.053 to 0.29. The mean value was 0.122, with a standard deviation of 0.039. The depth-to-diameter ratios were found to be concentrated in the range from 0.07 to 0.17, with more than 80% of the ratios falling within this range. Furthermore, and 50% of the impact craters exhibited depth-to-diameter ratios between 0.10 and 0.16. Both studies demonstrate a linear relationship between depth and diameter. The findings of this study align with those of previous research, indicating that the methodology and process employed in this study are highly reliable. However, the impact crater diameters were found to be larger and the depth-to-diameter ratios smaller than in previous studies. This was due to the larger number of impact craters counted in this study than in previous studies, which provided more accurate statistical analyses for studying the sub-metre impact craters.

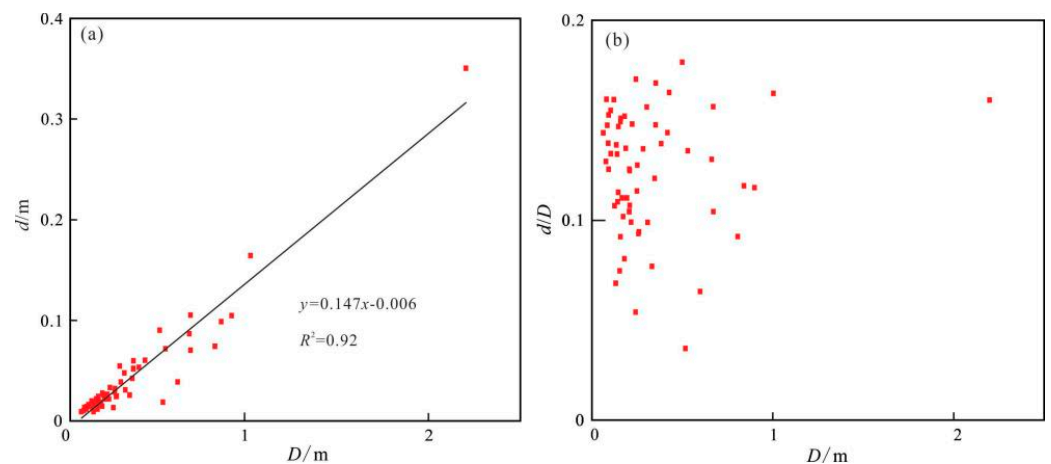


Figure 15. Results of the existing study. (a) shows a plot of diameter versus depth, and (b) shows a plot of diameter versus depth-to-diameter ratio.

4.2. Statistical Patterns of Regional Population of Micro-Impact Craters

The image data obtained from the landing zone of Chang'e-4 [22] and the image data collected along the rover's route were subjected to a comparative analysis in order to identify the statistical patterns present in the population of the small impact crater craters observed in the lunar back region. Firstly, both studies demonstrated an inverse relationship between the impact crater size and frequency. This inverse relationship can be described as follows: the smaller the impact crater was, the higher the frequency was, and the larger the impact crater size was, the lower the frequency was. Regarding the distributions, the landing camera's come-centre landing zone exhibited a higher image

ground resolution, with 975 impact craters with diameters ranging from 0.15 to 0.5 m in the 30 m range around the landing site. However, due to the limitations of the image resolution, the peripheral zones prevented the further extraction and identification of miniature impact craters. The resolution of the panoramic camera's close observation was sufficient to reach the millimetre level, which enabled the extraction of a greater number of smaller-sized impact craters. Nevertheless, it proved challenging to identify and extract impact craters with diameters exceeding 2 m due to the limitations of the panoramic camera's shooting imaging angle and height. In conclusion, a greater number of impact craters with diameters below 1 m were identified in the landing zone and along the rover's route, indicating a high density of impact craters.

With regard to the level of degradation, 6316 impact craters were extracted from the landing zone, with only 19 identified as fresh impact craters with a minimum diameter greater than 2 m. In contrast, 2015 impact craters were extracted along the rover's route, with no fresh impact craters observed. A mere 2.99% of the impact craters in the landing zone exhibited slight degradation, while 99.7% were severely degraded to varying degrees. The remaining 96.71% were moderately degraded or severely degraded. The proportion of severely degraded craters gradually increased as the size of the craters decreased, while the proportion of fresh craters gradually increased as the size of the craters increased. In parallel, all impact craters along the rover's route exhibited varying degrees of degradation, with 6% classified as moderately degraded. The results of the two studies indicate that the degradation of small impact craters in the region was significant. Nevertheless, 87 moderately degraded impact craters with diameters ranging from 0.1 to 1 m were identified along the rover's route, reflecting the ease with which such craters can be formed and degraded.

4.3. Analysis of Impact Crater Impact Saturation

As the number of impact craters continues to increase, the density of impact craters will eventually reach an upper limit [12,23], particularly for smaller-diameter craters. A cluster of smaller impact craters below a certain diameter is considered saturated when the rate of their creation is equal to the rate of their degradation [24]. The method of saturating the density of impact craters with empirical assessment, as proposed by Gault (1970) [25] and Hartmann (1984) [26], is a widely used approach. In this study, the CraterStats2 tool was used to plot the Hartmann saturation line of impact craters in the 10-station studied area, as illustrated in Figure 16. Figure 14 illustrates a clear inflexion point at 0.2 m, which is evident in the impact crater. A power law fit to the impact craters in the region was performed using Clausi et al. (1970)'s technique [25] to obtain cumulative SFD slopes and equilibrium onset diameters, as shown in Table 2. The cumulative SFD slope of the impact crater population at equilibrium from decimetres to hundreds of meters was -2 , while the production slope was -3 . This indicates that the impact craters in the study region were not saturated. The area traversed by the Yutu-2 rover's route may be of greater antiquity, exhibiting thicker weathering layers [27]. Therefore, several secondary impact craters may be distributed, which are more likely to be widely distributed in the sub-metre diameter range. Furthermore, smaller impact craters are challenging to saturate with impact craters due to their high probability of new cratering and greater likelihood of burial by ejecta from neighbouring impact craters.

Table 2. Saturation of impact craters in the statistical region.

Counting Areas	Cumulative SFD Slopes of Crater Population in Equilibrium	D_{eq} (m)
Area along the rover's route	-3.6898	0.8177

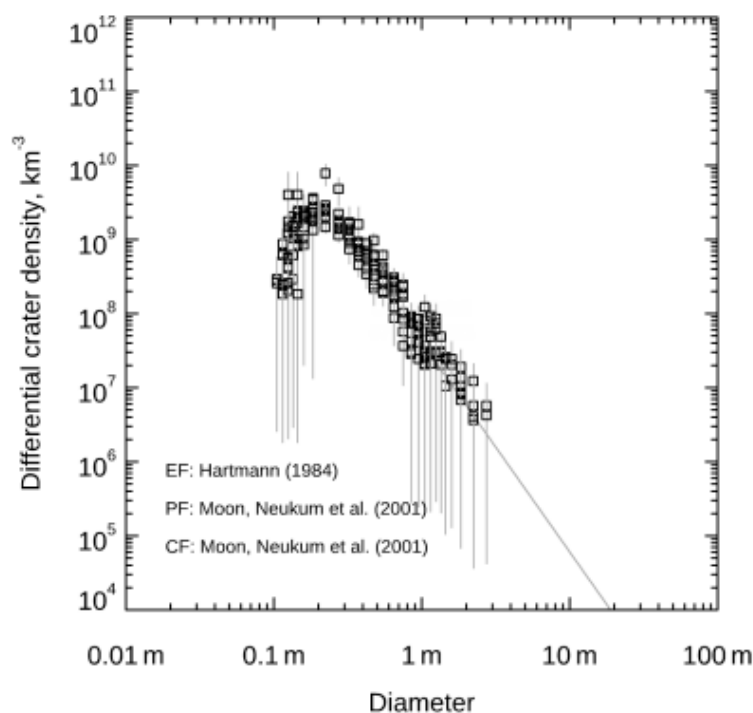


Figure 16. Craterstats2 programme-calculated equilibrium lines [26,28].

5. Conclusions

In this paper, we synthesized and analysed 2015 impact craters with diameters ranging from 0.08 to 4.07 m in panoramic camera images from the 27th to 33rd lunar days, alongside their morphological parameters and degradation levels. Our findings led to the following conclusions:

- (1) The majority of the impact craters had diameters between 0.1 and 2 m, with the number of impact craters observed to decrease with increasing size. The distribution of the impact crater depth-to-diameter ratios exhibited a range from 0.053 to 0.29, with over 80% of the minor impact craters exhibiting depth-to-diameter ratios within the range from 0.07 to 0.17.
- (2) A negative correlation was observed between the depth-to-diameter ratios and the diameters of minor impact craters. This correlation exhibited a decreasing trend in the depth-to-diameter ratio and a decreasing trend in the population degradation with increasing size.
- (3) The area and impact craters along the rover's route exhibited severe degradation overall, with the groups' degradation degree progressively decreasing with increasing diameter.
- (4) The achievement of saturation was challenging due to the high probability of the emergence of new craters emerging from sub-metre-scale (mainly below 2.0 m in diameter) impact craters and the high probability of burial by spatter.

The images captured by the Yutu-2 rover's panoramic camera can be used to compare and analyse the distribution and degradation of minor impact craters at the front and back of the moon. This will enable the exploration of the degradation and morphological parameter distribution laws of the impact crater population on the lunar surface.

Author Contributions: Conceptualisation, T.H. and Z.K.; data curation, X.M. and M.C.; formal analysis, X.M. and M.C.; methodology, T.H.; software, M.X.; visualisation, X.M.; writing—original draft, X.M. and M.C.; writing—review and editing, X.M., M.C. and T.H. All authors have read and agreed to the published version of the manuscript.

Funding: This work was supported by the National Natural Science Foundation of China (grant no. 41602215), the National Key Research and Development Program of China (2019YFE0123300),

and a pre-research project on Civil Aerospace Technologies (D020204) funded by the China National Space Administration (CNSA). 2023 University Students' Innovation and Entrepreneurship Training Project of China University of Geosciences, Beijing (S202311415157).

Data Availability Statement: The original contributions of this study are included in this article. Further inquiries can be directed to the corresponding authors.

Acknowledgments: We express our thanks to the “Ground Research and Application System (GRAS) of China’s Lunar and Planetary Exploration Program, provided by China National Space Administration (<http://moon.bao.ac.cn>)” for providing the data set used in this study.

Conflicts of Interest: The authors declare no conflicts of interest.

References

- Ou Yang, Z.Y.; Li, C.L.; Zou, Y.Y.; Liu, J.Z. Progress of scientific application and research of China’s circumlunar exploration program. *Bull. Chin. Acad. Sci.* **2009**, *24*, 530–536.
- Lin, H.; Chen, J.; Li, C.; Ding, C.; Xiao, X.; Huang, J.; Ji, J.; Gou, S.; Zhang, J.; Wei, Y.; et al. Research progress of remote sensing for the Chang’E lunar exploration mission. *Bull. Mineral. Petrol. Geochem.* **2023**, *42*, 478–493.
- Michael, G.G.; Neukum, G. Planetary surface dating from crater size-frequency distribution measurements: Partial resurfacing events and statistical age uncertainty. *Earth Planet. Sci. Lett.* **2010**, *294*, 223–229. [[CrossRef](#)]
- Yue, Z.Y.; Shi, K.; Di, K.C.; Lin, Y.T.; Gou, S. Progresses and prospects of impact crater studies. *Sci. China-Earth Sci.* **2023**, *66*, 2441–2451. [[CrossRef](#)]
- Prieur, N.C.; Rolf, T.; Wünnemann, K.; Werner, S.C. Formation of Simple Impact Craters in Layered Targets: Implications for Lunar Crater Morphology and Regolith Thickness. *J. Geophys. Res.-Planets* **2018**, *123*, 1555–1578. [[CrossRef](#)]
- Sun, S.J.; Yue, Z.Y.; Di, K.C. Investigation of the depth and diameter relationship of subkilometer-diameter lunar craters. *Icarus* **2018**, *309*, 61–68. [[CrossRef](#)]
- Craddock, R.A.; Howard, A.D. Simulated degradation of lunar impact craters and a new method for age dating farside mare deposits. *J. Geophys. Res.-Planets* **2000**, *105*, 20387–20401. [[CrossRef](#)]
- Haruyama, J.; Ohtake, M.; Matsunaga, T. Detectability of Degradation of Lunar Impact Craters by SELENE Terrain Camera. *ResearchGate* **2004**, *3*, 1496.
- Wood, C.; Head, J.; Cintala, M. Crater Degradation on Mercury and the Moon: Clues to Surface Evolution. 1977. Available online: <https://adsabs.harvard.edu/full/1977LPSC...8.3503W> (accessed on 25 April 2024).
- Ivanov, M.; Basilevsky, A. Morphology and Size–Frequency Distribution of Kilometer-Scale Impact Craters on Callisto and Ganymede Derived from Galileo Data. *Sol. Syst. Res.* **2002**, *36*, 447–457. [[CrossRef](#)]
- Hartmann, W.K.; Gaskell, R.W. Planetary cratering 2: Studies of saturation equilibrium. *Meteorit. Planet. Sci.* **1997**, *32*, 109–121. [[CrossRef](#)]
- Richardson, J.E. Cratering saturation and equilibrium: A new model looks at an old problem. *Icarus* **2009**, *204*, 697–715. [[CrossRef](#)]
- Li, K. Study on Small-Scale Lunar Craters’ Morphology and Degradation. Ph.D. Thesis, Wuhan University, Wuhan, China, 2013.
- Arthur, D.; Agnieray, A.; Horvath, R.; Wood, C.; Chapman, C. The System of Lunar Craters, Quadrant I. *Commun. Lunar Planet Lab.* **1964**, *2*, 71–78.
- Mcgill, G.E.; Wise, D.U. Regional variations in degradation and density of Martian craters. *J. Geophys. Res.* **1972**, *77*, 2433–2441. [[CrossRef](#)]
- Basilevskii, A.T. On the evolution rate of small lunar craters. *Lunar Planet. Sci. Conf. Proc.* **1976**, *1*, 1005–1020.
- Yao, M.J.; Chen, J.P.; Wang, X.; Xu, B. The grading and evolution analysis of lunar crater based on optimum partition and grading method. *Acta Petrol. Sin.* **2016**, *32*, 119–126.
- Ground Research and Application System of China’s Lunar and Planetary Exploration Program. Chang’E 4 Panoramic Cameras Dataset. China National Space Administration. 2020. Available online: <http://moon.bao.ac.cn> (accessed on 20 February 2023).
- Dai, S.; Wu, J.; Sun, H.; Zhang, B.; Yang, J.; Fang, G.; Wang, J.; Wang, H.; An, J. Chang’E-3 Lunar Rover’s Scientific Payloads. *Chin. J. Space Sci.* **2014**, *34*, 332–340. [[CrossRef](#)]
- Jia, Y.; Zou, Y.; Xue, C.; Ping, J.; Yan, J.; Ning, Y. Scientific Objectives and Payloads of Chang’E-4 Mission. *Chin. J. Space Sci.* **2018**, *38*, 118–130. [[CrossRef](#)]
- Yang, M.; Yue, Z.; Di, K.; Wan, W.; Liu, J.; Shi, K. Statistical Analysis of Secondary Craters in the Chang’E-4 Landing Area Based on Panoramic Camera Data. *Bull. Mineral. Petrol. Geochem.* **2021**, *40*, 720–729.
- Hu, T.; Yang, Z.; Kang, Z.Z.; Lin, H.Y.; Zhong, J.; Zhang, D.Y.; Cao, Y.M.; Geng, H.M. Population of Degrading Small Impact Craters in the Chang’E-4 Landing Area Using Descent and Ground Images. *Remote Sens.* **2022**, *14*, 3608. [[CrossRef](#)]
- Melosh, H.J. Impact Cratering: A Geologic Process. *Geol. Mag.* **1989**, *126*, 729–730. [[CrossRef](#)]
- Xiao, Z.Y.; Werner, S.C. Size-frequency distribution of crater populations in equilibrium on the Moon. *J. Geophys. Res.-Planets* **2015**, *120*, 2277–2292. [[CrossRef](#)]
- Gault, D.E. Saturation and Equilibrium Conditions for Impact Cratering on the Lunar Surface: Criteria and Implications. *Radio Sci.* **1970**, *5*, 273–291. [[CrossRef](#)]
- Hartmann, W.K. Does crater “saturation equilibrium” occur in the solar system? *Icarus* **1984**, *60*, 56–74. [[CrossRef](#)]

-
27. Qiao, L.; Ling, Z.H.; Fu, X.H.; Li, B. Geological characterization of the Chang'e-4 landing area on the lunar farside. *Icarus* **2019**, *333*, 37–51. [[CrossRef](#)]
 28. Neukum, G.; Ivanov, B.; Hartmann, W.K. Cratering records in the Inner solar system in relation to the lunar reference Space. *Sci. Rev.* **2001**, *96*, 55–86.

Disclaimer/Publisher's Note: The statements, opinions and data contained in all publications are solely those of the individual author(s) and contributor(s) and not of MDPI and/or the editor(s). MDPI and/or the editor(s) disclaim responsibility for any injury to people or property resulting from any ideas, methods, instructions or products referred to in the content.